

Donor-acceptor conjugated copolymer with high thermoelectric performance: A case study of the oxidation process within chemical doping

Liangjun Chen(陈凉君), Wei Wang(王维), Shengqiang Xiao(肖生强), and Xinfeng Tang(唐新峰)
Citation: Chin. Phys. B, 2022, 31 (**2**): 028507. DOI: 10.1088/1674-1056/ac3504
Journal homepage: http://cpb.iphy.ac.cn; http://iopscience.iop.org/cpb
What follows is a list of articles you may be interested in

Structure design for high performance n-type polymer thermoelectric materials

Qi Zhang(张奇), Hengda Sun(孙恒达), and Meifang Zhu(朱美芳)
Chin. Phys. B, 2022, 31 (**2**): 028506. DOI: 10.1088/1674-1056/ac3a64

Gas sensor using gold doped copper oxide nanostructured thin films as modified cladding fiber

Hussein T. Salloom, Rushdi I. Jasim, Nadir Fadhil Habubi, Sami Salman Chiad, M Jadan, and Jihad S. Addasi
Chin. Phys. B, 2021, 30 (**6**): 068505. DOI: 10.1088/1674-1056/abd2a7

Cathodic shift of onset potential on TiO_2 nanorod arrays with significantly enhanced visible light photoactivity via nitrogen/cobalt co-implantation

Xianyin Song(宋先印), Hongtao Zhou(周洪涛), and Changzhong Jiang(蒋昌忠)
Chin. Phys. B, 2021, 30 (**5**): 058505. DOI: 10.1088/1674-1056/abee07

Vertical polarization-induced doping InN/InGaN heterojunction tunnel FET with hetero T-shaped gate

Yuan-Hao He(何元浩), Wei Mao(毛维), Ming Du(杜鸣), Zi-Ling Peng(彭紫玲), Hai-Yong Wang(王海永), Xue-Feng Zheng(郑雪峰), Chong Wang(王冲), Jin-Cheng Zhang(张进成), and Yue Hao(郝跃)
Chin. Phys. B, 2021, 30 (**5**): 058501. DOI: 10.1088/1674-1056/abd73f

A new algorithm based on *C-V* characteristics to extract the epitaxy layer parameters for power devices with the consideration of termination

Jiupeng Wu(吴九鹏), Na Ren(任娜), and Kuang Sheng(盛况)
Chin. Phys. B, 2021, 30 (**4**): 048505. DOI: 10.1088/1674-1056/abcf9e

---

SPECIAL TOPIC — Organic and hybrid thermoelectrics

Donor-acceptor conjugated copolymer with high thermoelectric performance: A case study of the oxidation process within chemical doping

Liangjun Chen(陈凉君)[†], Wei Wang(王维)[†], Shengqiang Xiao(肖生强)[‡], and Xinfeng Tang(唐新峰)[§]

State Key Laboratory of Advanced Technology for Materials Synthesis and Processing, Wuhan University of Technology, Wuhan 430070, *China*

(Received 22 September 2021; revised manuscript received 25 October 2021; accepted manuscript online 1 November 2021)

The doping process and thermoelectric properties of donor-acceptor (D-A) type copolymers are investigated with the representative poly([2,6′-4,8-di(5-ethylhexylthienyl)benzo[1,2-b;3,3-b] dithiophene]3-fluoro-2-[(2-ethylhexyl)-carbonyl]thieno[3,4-b]thiophenediyl)) (PTB7-Th). The PTB7-Th is doped by $FeCl_3$ and only polarons are induced in its doped films. The results reveal that the electron-rich donor units within PTB7-Th lose electrons preferentially at the initial stage of the oxidation and then the acceptor units begin to be oxidized at a high doping concentration. The energy levels of polarons and the Fermi level of the doped PTB7-Th remain almost unchange with different doping levels. However, the morphology of the PTB7-Th films could be deteriorated as the doping levels are improved, which is one of the main reasons for the decrease of electrical conductivity at the later stage of doping. The best electrical conductivity and power factor are obtained to be 42.3 $S{\cdot}cm^{-1}$ and 33.9 $\mu W{\cdot}mK^{-2}$, respectively, in the doped PTB7-Th film at room temperature. The power factor is further improved to 38.3 $\mu W{\cdot}mK^{-2}$ at 75 °C. This work may provide meaningful experience for development of D-A type thermoelectric copolymers and may further improve the doping efficiency.

Keywords: donor-acceptor copolymer, doping, oxidization process, thermoelectric performance

PACS: 85.30.De, 72.80.Le **DOI:** 10.1088/1674-1056/ac3504

1. Introduction

Thermoelectric technology has gained extensive attention for several decades as a clean energy technology that can convert waste heat energy into electricity directly.[1–4] Recently, with the growing demand for organic thermoelectric devices in wearable next-generation electronic devices, conjugated polymers have shown great potential in thermoelectric applications at moderate temperatures. Because conjugated polymers have advantages such as flexibility, light-weight, good thermal stability, and mechanical properties for applications.[5,6] ZT or power factor (PF) is usually adopted to measure the thermoelectric performance of conjugated polymers, both of which have a positive correlation with their Seebeck coefficient (S) and electrical conductivity (σ).[7] Among the few reported classes of conjugated polymers, p-type homopolymers, represented by poly(3,4-ethylenedioxythiophene) (PEDOT) and poly(3-hexylthiophene) (P3HT), are the lead ones in the thermoelectric performance.[8] To date, the thermoelectric devices based on PEDOT/Bi_2Te_3 have provided the highest ZT up to 0.58 at room temperature.[9] However, some intrinsic properties determined by their chemical structure limit their further development, such as the hygroscopic nature and counterion effects of PEDOT:poly(styrene sulfonate) (PEDOT:PSS) and the untunable wide bandgap (1.9–2.0 eV) of P3HT.[10,11]

As an alternative class of conjugated polymers for the thermoelectric application, a donor-acceptor (D-A) type conjugated copolymer typically consists of an electron-rich donor unit and an electron-deficient acceptor unit. The energy state (e.g., energy band and levels) and aggregation behavior (e.g., molecular packing orientation and ordering) of a D-A type copolymer can be tuned flexibly by molecular engineering as the needs.[12–15] The chemical structure optimization has therefore become one of the effective means to develop high-performance D-A type copolymers in thermoelectric application.[8,16–18] For instance, Woo *et al.* designed and synthesized a D-A type conjugated copolymer named PCPDTSBT by replacing the alkyl side-chains in poly[(4,4′-bis(2-ethylhexyl)cyclopenta[2,1-b:3, 4-b′]dithiophene)-alt-(benzo[c][1,2,5] thiadiazole)] (PCPDTBT) with bis(alkylsulfanyl)-methylene substituents. The extended chain planarity and the sulfur-sulfur (S-S) chalcogen interactions lead to the improved molecular packing and crystallinity of PCPDTSBT. When doped with the Lewis acid $B(C_6F_5)_3$, PCPDTSBT presented ∼1 order higher optimized σ (7.47 $S{\cdot}cm^{-1}$) than that of PCPDTBT (0.65 $S{\cdot}cm^{-1}$) with asuperior PF of 7.73 $\mu W{\cdot}m^{-1}{\cdot}K^{-2}$ at room temperature.[19] Although some progress has been made in D-A type thermoelectric copolymers, their performance is still lagging behind the homopolymers like P3HT and PE-

[†]Liangjun Chen and Wei Wang contributed equally to this work.
[‡]Corresponding author. E-mail: shengqiang@whut.edu.cn
[§]Corresponding author. E-mail: tangxf@whut.edu.cn

© 2022 Chinese Physical Society and IOP Publishing Ltd

DOT. On the one hand, it could be attributed that there are only a few D-A type copolymers that have been successfully applied in thermoelectrics, which limits bringing the potential of such copolymers into play. On the other hand, the doping of such D-A type copolymers has not been fully explored yet. Doping plays a critical role in improving the σ of conjugated polymers, which is essentially a redox reaction. When subjected to the oxidation process, the same units in a p-type homopolymer (e.g. P3HT) have the almost equivalent ability to lose an electron. However, the donor and acceptor units within a copolymer have quite a different electronegativity, generally inducing the formation of a charge transfer complex within the copolymer.[20] It may result in a complicated oxidation process and evolution of electric structures in D-A type copolymers during doping. Understanding such doping processes in D-A type copolymers clearly is conducive to carry out the targeted chemical structure optimization and to improve the doping efficiency.

In this work, the representative two-dimensional (2D) D-A type copolymer, poly([2,6′-4,8-di(5-ethylhexylthienyl)benzo[1,2-b;3,3-b]dithiophene]3-fluoro-2-[(2-ethylhexyl)-carbonyl]thieno[3,4-*b*]thiophenediyl) (PTB7-Th) was chosen to investigate the thermoelectric performance and doping process of the D-A type copolymers for the first time due to its great potential in the thermoelectric application. The thienyl alkane side chains in PTB7-Th lead to the extended conjugated plane and better interchain π–π overlapping, and thus PTB7-Th could offer higher carrier mobility than its one-dimensional counterparts with linear alkyl side chains (PTB7).[21,22] In addition, the electron-rich thiophenes in the side chains narrow the bandgap of PTB7-Th to 1.59 eV from 1.84 eV of PTB7, which has been suggested to be beneficial to obtain a better Seebeck coefficient.[16,23–25] The p-type chemical doping of PTB7-Th was performed by immersing its film with an oxidant solution of $FeCl_3$ in nitromethane. The results reveal that oxidation does not occur simultaneously on the donor units and the acceptor units when doping PTB7-Th while the donor units lose electrons earlier and more quickly than the acceptor units. The σ of the doped PTB7-Th arrives at 42.3 S·cm^{-1} at room temperature while the room temperature S remains $\sim$ 90 μV·K^{-1} in the high doping levels. The highest PFs of 33.9 and 38.3 μW·mK^{-2} are obtained in the doped PTB7-Th films at room temperature and 75 °C, respectively.

2. Experimental details

2.1. Materials

PTB7-Th was synthesized via palladium-catalyzed Stille cross-coupling polycondensation reactions between (4,8-bis(5-(2-ethylhexyl)thiophen-2-yl)-benzo [1,2-b:4,5-b′]dithiophene-2,6-diyl)bis(trimethylstannane) (BDTT) and 2-ethylhexyl -4,6-dibromo-3-fluorothieno[3,4-b]thiophene-2-carboxylate (FTT). BDTT (98%) and FTT (98%) adopted in this work were purchased from Derthon. The detailed synthetic procedure was described in our previous publication.[23] The number-average molecular weights (M_n) of PTB7-Th was 22618 g·mol^{-1} with a PDI of 2.22. Ethanol (AR, 99.7%), acetone (AR, 99.5%), and isopropanol (AR, 99.7%), and nitromethane (CP, 98.5%) were purchased from Sinopharm. Superdry chlorobenzene (99.8%) was purchased from J&K. Anhydrous $FeCl_3$ (AR, 99%) were purchased from MACKLIN. All of the chemicals were used without further purification.

2.2. Device fabrication

Glass substrates (2 cm×2 cm) were cleaned in deionized water, ethanol, acetone, and isopropanol sequentially with ultrasound assists and then the substrates were blown dry with nitrogen. The substrates were then further cleaned by UV-ozone for 10 min before using. PTB7-Th was dissolved in chlorobenzene with a concentration of 25 mg·mL^{-1}. A PTB7-Th film was obtained by spin-coating on the glass substrate at 1000 rpm for 1 min. The as-prepared films were dried naturally in ambient air. Anhydrous $FeCl_3$ was dissolved in nitromethane with a concentration of 0.01 mol·L^{-1}. The PTB7-Th films were immersed in the $FeCl_3$ solution for a specified time, rinsed with nitromethane, and subsequently blown dried with nitrogen before being transferred instantly to a measurement system. The humidity in air was controlled at 30%–40% during processing.

2.3. Characterization

The molecular weight of PTB7-Th was determined by gel permeation chromatography (GPC). The thermogravimetry (TG) analysis was carried out on a NETZSCH thermogravimetric analyzer (STA449F3) at a heating rate of 10 °C·min^{-1} under nitrogen. UV-vis absorption spectra were measured on a Shimadzu UV-1750 spectrophotometer. UV-vis-NIR absorption spectra were obtained on a Lambda 750 S spectrophotometer. Cyclic voltammogram (CV) measurements were carried out in a solution of 0.1 mol·L^{-1} tetrabutylammonium hexafluorophosphate (Bu_4NPF_6) in anhydrous acetonitrile as the supporting electrolyte on a CHI605E electrochemical analyzer. Raman spectra were collected on a LabRAM HR Evolution Raman Spectrometer using a 532 nm laser (Horiba Scientific). The film morphology was characterized by a field emission scanning electron microscope (FESEM, Hitachi SU8020). The thickness of films was measured on a stylus profiler (DEKTAK-XT). The chemical valence of elements was determined using x-ray photoelectron spectroscopy (XPS) (ESCALAB 250Xi). The work function was measured with the aid of ultraviolet photoemission spectroscopy (UPS) (VG MultiLab 2000), and the Fermi level was set to 0 through the calibration of the gold sheet. The grazing incident wide-angle x-ray scattering (GIWAXS) measurements were carried out

with an Xeuss 2.0 SAXS/WAXS laboratory beamline using a Cu x-ray source (8.05 keV, 1.54 Å) and a Pilatus3R 300K detector. The electrical conductivity and the Seebeck coefficient of the films were measured simultaneously by a four-point method under helium atmosphere utilizing a commercial ULVAC-RIKO ZEM-3 apparatus.

3. Results and discussion

3.1. Material characterization

The thermal, optical, and electrochemical properties of PTB7-Th have been measured and the results are summarized in Table S1 in the supplementary information. Thermogravimetric analysis indicates that PTB7-Th is of good thermal stability. As presented in Fig. S1, there is almost no mass change detected for PTB7-Th when the temperature is lower than 300 °C and the decomposition temperature (T_d, 5% weight loss) of PTB7-Th is up to 369.6 °C under N_2 atmosphere. The UV-vis absorption spectra of PTB7-Th in a chlorobenzene solution (with 1×10^{-5} mg·mL^{-1}) and a film are depicted in Fig. S2 in the supplementary information. The absorption of PTB7-Th film is mainly located from 450 to 750 nm with the highest absorbance peak at 711 nm. The optical band gap ($E_{g,opt}$) of PTB7-Th was 1.58 eV derived from its absorption onset (784 nm) in the film. The highest occupied molecular orbital (HOMO) energy level (−5.23 eV) of PTB7-Th was calculated from the oxidation onset potential (0.531 V vs ferrocene) determined by cyclic voltammetry (Fig. S3). The lowest unoccupied molecular orbital (LUMO) energy level was estimated to be −3.64 eV according to $E_{LUMO} = (E_{HOMO} + E_{g,opt})$ eV.

3.2. Mechanism of chemical doping PTB7-Th

Upon chemical doping, polarons and bipolarons have been proposed to be the dominant two possible kinds of charge carriers in a conjugated polymer, and new electronic levels in the gap between HOMO and LUMO levels are created.[26–28] This charge carriers state in doped conjugated polymers is usually described as doping level.[29,30] UV-vis-NIR measurement was firstly carried out on the doped PTB7-Th films to investigate the nature of the charge carriers. Depicted in Fig. 1 are the UV-vis-NIR spectra of the PTB7-Th films with different doping levels, obtained by immersing them in an oxidant nitromethane solution of $FeCl_3$ (with 0.01 mol·L^{-1}) over a different time at room temperature. The undoped PTB7-Th film shows a strong absorption peak at 651 nm (peak I) with a shoulder peak at 711 nm (peak Ⅱ). For PTB7-Th, peak I is attributed to the π–π^* transitions on the conjugated backbones of PTB7-Th while peak Ⅱ is derived from the intermolecular interaction and ordering of PTB7-Th.[20,31] When doped for 30 s, a new absorption peak appears around 1119 nm (peak Ⅲ). As the doping time increases to 45 min, peak Ⅲ shows an improving absorption intensity with an isosbestic point at 761 nm, suggesting that only polarons formed in this doping process.[32–35] Such an increase in the intensity of peak Ⅲ is a manifestation of higher doping levels.[36,37] In addition, peaks I and Ⅱ both show a rapid decrease of absorption intensity while peak Ⅱ takes an obvious blueshift in the doping process. It hints that the chemical doping in PTB7-Th could weaken both the π–π^* transitions on its conjugated backbones and its structural ordering.

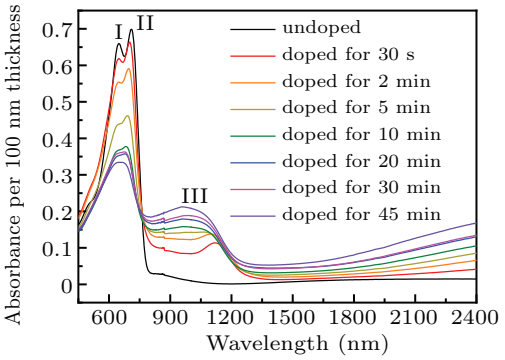


Fig. 1. UV-vis-NIR spectra of the PTB7-Th films immersed in 0.01 mol·L^{-1} solution of $FeCl_3$ in nitromethane for a different time at room temperature.

To reveal the effect of doping on the electronic structure of PTB7-Th, UPS analysis was performed to calculate the work function of the PTB7-Th with different doping levels (Fig. 2(a)). The work function can be calculated according to $\varphi = h\nu - (E_{cutoff} - E_{Fermi})$. In the PTB7-Th film immersed for 30 s, its E_{cutoff} is estimated to be 16.39 eV. As the immersion time increases, the E_{cutoff} of the doped PTB7-Th almost remains unchanged. When the immersion time is up to 45 min, the E_{cutoff} of the doped PTB7-Th moves slightly towards the lower binding energy for only 0.02 eV. The work functions of the doped PTB7-Th films immersed for 30 s, 10 min, and 45 min thus could be determined to be 4.81, 4.81, and 4.83 eV, respectively. Their corresponding Fermi levels could be obtained, which are quite close (Fig. 2(b)). Moreover, the appearance of peak Ⅲ in the PTB7-Th films with different doping levels proved that the formation of polarons changes the electronic transitions in the PTB7-Th film.[36,37] Such peaks in the UV-vis-NIR spectra correspond to the transition from the lower subgap level (ω_0) to the higher subgap level (ω_0^*) of the doped PTB7-Th.[29,38] The energy levels of polarons can be calculated from the absorption onset of the corresponding peak Ⅲ and the calculated results are presented in Fig. 2(b).[26,30,38] With the increasing immersion time from 30 s to 45 min, the relative energy of the higher subgap maintains at −3.93 eV while the lower subgap is located at −4.94 eV to −4.95 eV in the doped PTB7-Th. In brief, it can be concluded that chemical doping gives rise to the polaron level in PTB7-Th but the polaron level stays almost unchanged with the improving doping levels, and so do their Fermi levels.

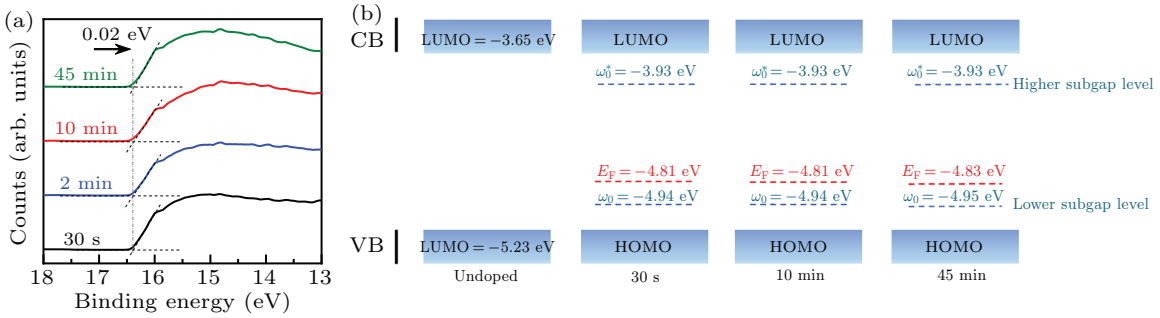


Fig. 2. Secondary electron cutoff region (a) and the energy level diagram (b) of the PTB7-Th films immersed in 0.01 mol·L^{-1} nitromethane solution of $FeCl_3$ for a different time at room temperature.

The formation of polarons is inevitably accompanied by the distortion of the polymer backbone. As an easy and accessible way to study the backbone structure and the ordering of conjugated polymers, Raman spectrum was thus measured to reveal the structural characteristics evolution of PTB7-Th in the doping process (Fig. 3).[39–41] In the neutral PTB7-Th film, peak 1 (at 1470 cm^{-1}) and peak 2 (at 1504 cm^{-1}) correspond to stretching vibration mode (C=C) of free thiophenes and fused thiophene in BDTT units respectively (Fig. 3(b)). Peak 3 (at 1536 cm^{-1}) is a coupled vibration of stretching vibration (C=C) of fused thiophene in BDTT units to the stretching mode (C=C) of non-fluorinated thiophene in FTT units while peak 4 (at 1577 cm^{-1}) corresponds to the quadrant stretching mode coupled to the stretching mode (C=C) of fluorinated thiophene in FTT units.[23] As the doping levels increase, the doping treatment not only does present a shift of the positions of the Raman bands towards a lower frequency but also makes the stretching vibrations and quadrant stretching weaker. It may attribute to the shortened conjugation length in the doped PTB7-Th, resulting from the oxidation of the conjugation units in PTB7-Th during the doping process. When immersing the PTB7-Th film for 30 s, peak 2 and peak 3 both shift to 1500 cm^{-1} and 1534 cm^{-1}, respectively, while the Raman shifts of peaks 1 and 4 nearly remain unchanged. It implies that the donor units of BDTT in PTB7-Th were preferentially oxidized at the initial stage of the doping process and this oxidation mainly occurred on the fused rings of BDTT in the polymer backbone. As the immersion time increases to 2 and 5 min, there are almost no further shifts in peak 2 and 3. However, peak 1 obviously moves to the lower frequency with a weakened intensity, suggesting that the oxidation on free thiophenes in BDTT units occurred after immersing for 2 min. As the immersion time increases up to 10 min, peaks 2 and 3 further shift to 1499 cm^{-1} and 1532 cm^{-1}, respectively, with the weakened intensity of peak 4, suggesting that the acceptor units of FTT gets oxidized. After the immersion for 45 min, peaks 2 and 3 shift to 1496 cm^{-1} and 1531 cm^{-1}, respectively, while peak 4 almost disappears. Besides their decreasing intensity, these feature peaks also become broader with the increasing doping levels, suggesting their reduced structure ordering of PTB7-Th.[42] It is worth noting that the up-shifts of Raman bands have been observed in the degradation process of PTB7 when exposing it to light and oxygen.[43] The opposite shift trend of Raman bands suggests that chemical oxidation and degradation have different reaction mechanisms.

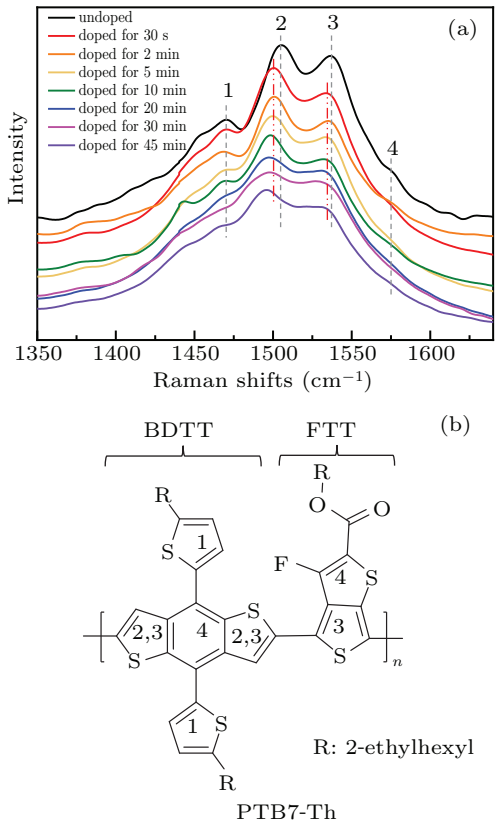


Fig. 3. Raman spectra of PTB7-Th films immersed in the 0.01 mol·L^{-1} nitromethane solution of $FeCl_3$ for a different time at room temperature.

To further reveal the oxidation process in the doped PTB7-Th film, XPS analysis was conducted to explore the chemical states of C and S elements in PTB7-Th at different doping levels for investigating their electron loss mechanism. Figure 4 shows the C (1s) core-level spectra of the PTB7-Th films with different doping levels. All binding energies were referenced to the neutral carbon C (1s) peak at 284.6 eV (284.6 eV was determined by the spectrometer).[44]

The C (1s) spectrum of neutral PTB7-Th features five components: C=C bond (at 284.1 eV),[45] C–C bond (at 284.6 eV), C–S bond (at 285.4 eV),[44] C–O bond (at 286.4 eV),[44,46] C–F, and O–C=O bond (at 288.9 eV).[47,48] The intensity ratio of C=C/C–C was calculated and summarized in Table 1. It could find that the intensity ratio of C=C/C–C decreases as the immersion time increases. It indicates that the C=C bonds in PTB7-Th have a higher priority for losing electrons during the oxidation process than the C–C bonds. In addition, the C (1s) (C-S bond) binding energy decreases to 285 eV with the oxidation of the C=C bonds. It hints that the electron cloud in C–S bond drifts towards the C atoms after the C=C bond loses electrons, which well explains the electron transfer from S atoms to the backbone.[49,50]

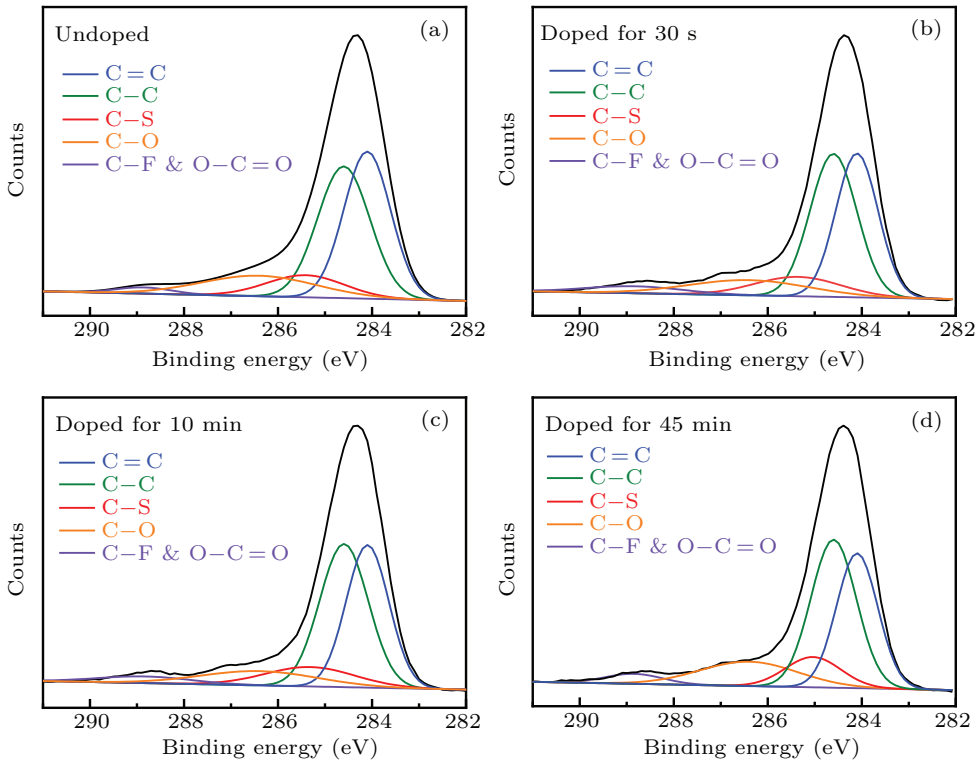


Fig. 4. C 1s core-level spectra for PTB7-Th films immersed in 0.01 mol·L^{-1} nitromethane solution of $FeCl_3$ for a different time at room temperature: (a) undoped (for 0 s), (b) for 30 s, (c) for 10 min, and (d) for 45 min.

Table 1. Intensity ratio of C=C/C–C at different doping levels.

Immersion time	0	30 s	10 min	45 min
Intensity ratio of C=C/C–C	1:1	0.91:1	0.88:1	0.83:1

The S (2p) core-level spectra for PTB7-Th films with different immersion time are presented in Fig. 5. The S (2p) electron binding energy of thiophene in the BDTT units is distinguished from that in the FTT units according to the disparity in electron-richness of thiophene units between donor and acceptor units.[47,48,51] The S (2p) electron binding energy in the donor part is denoted as S^1 and that in the acceptor part as S^2. The variation of S (2p) electron binding energy at different doping levels is summarized in Table 2. In a neutral PTB7-Th film, the peak of S^1 (2p 3/2) is located at 163.32 eV while the peak of S^2 (2p 3/2) is located at 163.91 eV. After immersing for 30 s, the peak S^1 (2p 3/2) moves to higher binding energy while the peak S^2 (2p 3/2) is still at 163.91 eV. It proves that the thiophene unit from the donor unit preferentially loses electrons at the initial stage of the oxidation process. When immersion time increases to 10 min, the peak S^1(2p 3/2) moves to 163.48 eV while the peak S^2 (2p 3/2) shows an obvious shift to 163.95 eV. It suggests that the thiophenes in the acceptor units start to lose electrons and those in the donor units were further oxidized. As the doping time increases to 45 min, the peak S^1 (2p 3/2) remains unchanged and the peak S^2 (2p 3/2) moves slightly to 163.97 eV. It implies that electron loss mainly occurs on the acceptor units in the later stage of doping. Given that acceptor units are less electron-rich than the donor units, it is more difficult for the thiophenes in the acceptor units to lose electrons during the oxidation process. Thus, the binding energy shifts of the peak S2 (2p 3/2) is much smaller than peak S1 (2p 3/2) in the oxidation process.

The oxidation process of the doped PTB7-Th can be described by the process shown in Fig. 6. The C=C bonds in fused thiophenes of donor units are the first to be oxidized by $FeCl_3$. A polaron corresponds to a positive charge on an oxidized unit. As the immersion time in the $FeCl_3$ solution prolongs, the increase of oxidized units in PTB7-Th resulted in its improving doping level. When the doping level reaches a

high level, the acceptor units in PTB7-Th began to be oxidized, which also happens on their C=C bonds of fused thiophenes. Such simultaneous oxidation in the donor and acceptor units would accelerate the increase of the doping level. In the later stage of doping, the oxidization in PTB7-Th mainly occurs in its acceptor units.

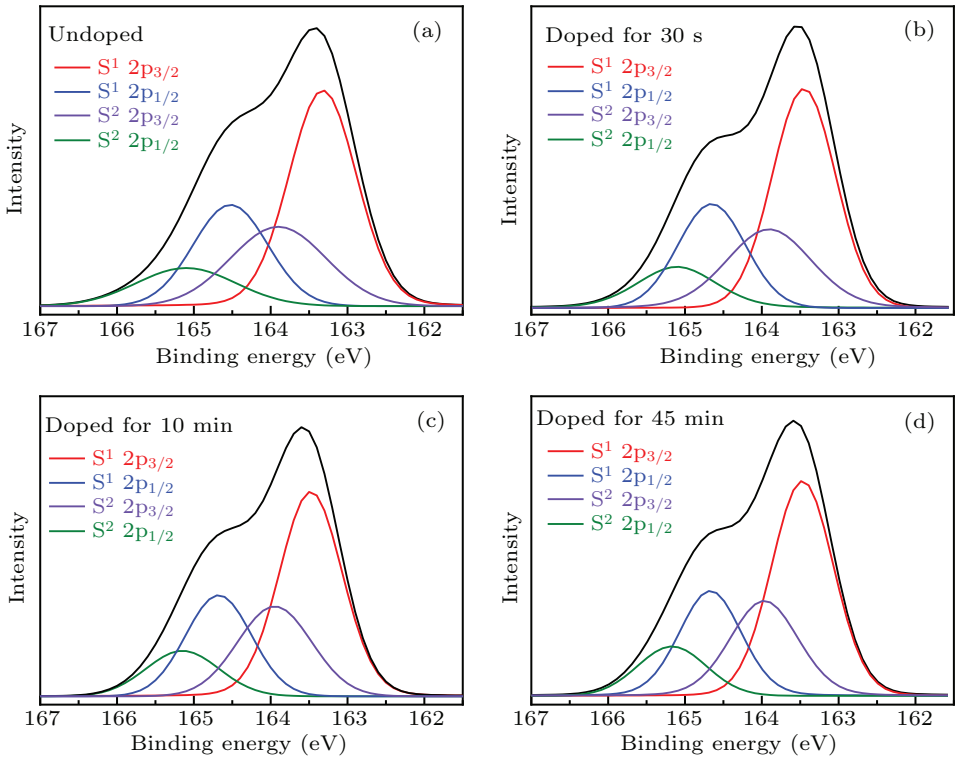


Fig. 5. S (2p) core-level spectra for PTB7-Th films immersed in 0.01 mol·L^{-1} solution of $FeCl_3$ in nitromethane for a different time at room temperature: (a) undoped (0 s), (b) 30 s, (c) 10 min, and (d) 45 min.

Table 2. Binding energy of S (2p) electron at different oxidation levels.

Immersion time	S^1 2p3/2	S^2 2p3/2	S^1 2p1/2	S^2 2p1/2
Undoped	163.32	163.91	164.52	165.11
30 s	163.45	163.91	164.65	165.11
10 min	163.48	163.95	164.68	165.15
45 min	163.48	163.97	164.68	165.17

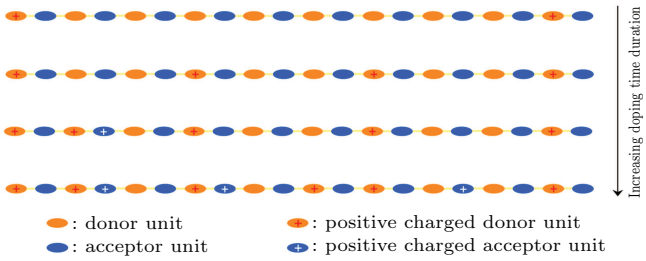


Fig. 6. Schematic diagram for the electron loss process of doping PTB7-Th with $FeCl_3$.

3.3. Morphology evolution in the doped PTB7-Th films

FESEM analysis was firstly carried out to figure out the effect of chemical doping on the surface of the PTB7-Th films. As shown in Fig. S4, the as-prepared neutral PTB7-Th film is smooth and flat but the nanoparticles appear on its film surface after being doped. Both the density and the size of such nanoparticles increase with the longer immersion time, which significantly enhances the surface roughness of the PTB7-Th films. When the PTB7-Th film is immersed for 45 min, the nanoparticles spread almost across its whole surface and the morphology deteriorates seriously, which is not conducive to efficient charge transfer. Furthermore, grazing incident wide-angle x-ray scattering (GIWAXS) was then adopted to investigate the evolution of molecular packing and structural ordering in the PTB7-Th films with different doping levels. The detailed GIWAXS characteristics have been summarized in Table S2. As shown in Fig. 7, the GIWAXS patterns indicated that the PTB7-Th films all present the preferable face-on orientated molecular packing, according to the (100) and (010) diffraction in the in-plane (IP) at $q_r = \sim 0.264$ Å^{-1} and in the out-of-plane (OOP) directions at $q_r = \sim 1.61$ Å^{-1}. The GIWAXS profiles and patterns of the neutral and doped PTB7-Th film do not show a remarkable difference in the initial doping stage. It means that the molecular packing and structural ordering of PTB7-Th are relatively stable during this oxidation period. As the immersion time increased to 45 min, the slightly higher q_r observed in OOP implies a closer π–π stacking adopted in this PTB7-Th film while its OOP (010) diffraction peak becomes broad and blunt. It suggests that the structural ordering and crystallinity of the PTB7-Th become worse with the increasing doping levels, which is consistent with the results in the UV-vis-NIR as well as Raman spectra.

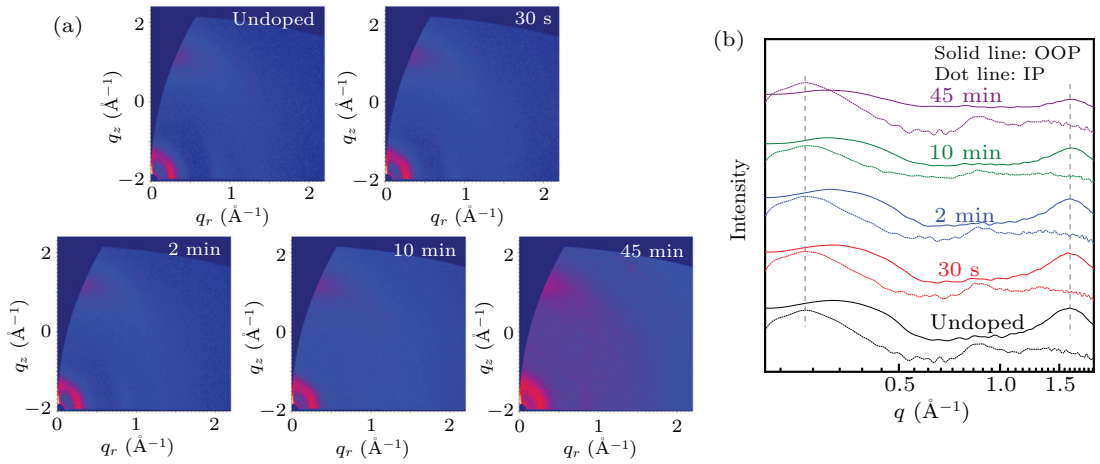


Fig. 7. GIWAXS profiles (a) and patterns (b) along the out-of-plane (OOP) and in-plane (IP) directions of the neutral and doped PTB7-Th films immersed in a 0.01 M $FeCl_3/CH_3NO_2$ solution for a different time.

3.4. Thermoelectric performance

The thermoelectric parameters σ, S, and PF of the PTB7-Th films with different doping levels were measured at room temperature (Fig. 8).

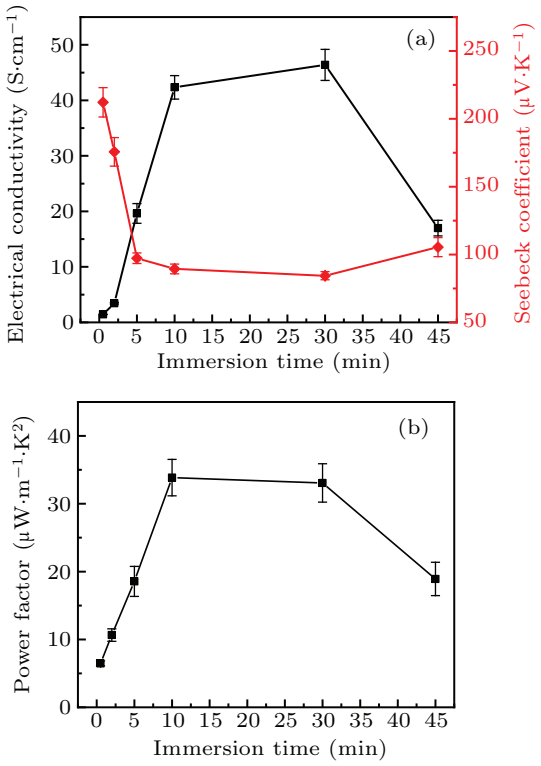


Fig. 8. (a) Electrical conductivity, Seebeck coefficient, and (b) power factor at room temperature of the PTB7-Th films immersed in 0.01 mol·L^{-1} nitromethane solution of $FeCl_3$ for a different time.

The σ increases dramatically from 1.44 to 42.3 S·cm^{-1} during the initial stage with the doping time from 30 s to 10 min. When the immersion time is 30 s, polaronic charge carriers in the PTB7-Th film were less mobile with a low doping concentration because they were trapped in the coulombic potential wells created by dopant counterions. When the higher doping concentration was realized in the sample immersed for 10 min, the coulombic potential wells began to overlap gradually, which reduces the energy barrier for polaronic transport and thus promotes the electrical conductivity. As the doping time increased to 30 min, the acceptor units in PTB7-Th were oxidized and the concentration of polarons arrived at a high level. The σ thus lowly increases and tends to saturations with the maximum of 46.4 S·cm^{-1}. Although the concentration of polarons remains at a high level with the doping time further increasing to 45 min, the σ rapidly decreases to 17.0 S·cm^{-1} as a result of the deterioration of the morphology and shortening of the conjugation length. The S presents an inverse trend to the σ with the increasing doping time. The S of the PTB7-Th film decreases initially from 212.2 μV·K^{-1} to 89.4 μV·K^{-1} with the doping time from 30 s to 10 min and then levels off as the doping time increases with the lowest S of 84.4 μV·K^{-1}. Finally, the highest PF of 33.9 μW·mK^{-2} was obtained in the PTB7-Th film immersed for 10 min at room temperature.

To explore the temperature-dependent thermoelectric transport properties of the doped PTB7-Th, the σ, S, and PF as a function of temperature were measured with the three representative samples (the PTB7-Th films doped for 2, 10, and 45 min, respectively). As presented in Fig. 9, the increasing temperature results in the decreasing σ of all three samples with a slow decline from 30 to 50 °C and an accelerated decline from 50 to 75 °C. It may indicate a heavily doped semiconducting behavior attributed to a change in carrier concentration.[52] As the temperature rises, the dedoping process could occur in these three samples, which results in their decreased doping levels and thus drops their carrier concentration.[53] The S of the three samples presents an opposite trend to σ with the increasing temperature. The sample with 10 min doping possesses the highest σ while the sample with 2 min doping possesses the highest S in the whole measured temperature range. The PF of the three samples improves steadily as the temperature rises. The PTB7-Th film

doped for 10 min offers the highest PF than the other two at every measured temperature and its PF tends to be stable when the temperature is over 50 °C. The highest PF thus reaches 38.3 μW·mK^{-2} at 75 °C in the PTB7-Th film doped for 10 min, enhancing from its PF of 33.9 μW·mK^{-2} at room temperature.

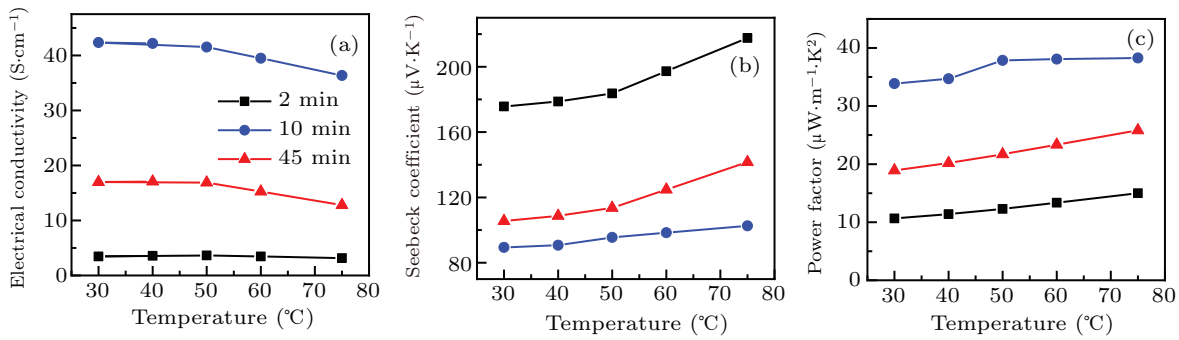


Fig. 9. Temperature-dependent (a) electrical conductivity, (b) Seebeck coefficient, and (c) power factor of the PTB7-Th films immersed in 0.01 mol·L^{-1} solution of $FeCl_3$ in nitromethane for 2 min, 10 min and 45 min.

4. Conclusions

In summary, we have systematically examined the oxidation mechanism of $FeCl_3$ doping in PTB7-Th and its effect on thermoelectric performance. At the early stage of doping, only the C=C bonds of fused thiophenes in the donor units lose their electron and the oxidization resulted in the formation of polarons. When the doping levels arrived at a high level, oxidation occurred in its acceptor units. This doping in PTB7-Th only induces polarons while the resulted energy levels of polarons and the Fermi level of the doped PTB7-Th remain unchanged with the increasing doping levels. However, the continuous deterioration is observed in the surface roughness and structural ordering of the PTB7-Th films as the doping time prolongs, which has a negative effect on the charge transfer and thus limits their further performance improvement. The σ of the PTB7-Th film increases to its maximum of 42.3 S·cm^{-1} after doping for 10 min while the S of the PTB7-Th with high doping levels maintains a high value of $\sim$ 90 μV·K^{-1} at room temperature. A high PF of 33.9 μW·mK^{-2} was also obtained in the PTB7-Th film immersed for 10 min at room temperature, which further improved to 38.3 μW·mK^{-2} at 75 °C. This work provides a case for understanding the doping process in D-A type copolymers, which is meaningful for optimizing their structure design and realizing the efficient doping for higher thermoelectric performance.

Acknowledgement

This work was supported by the National Key Research and Development Program of China (Grant No. Q2019YFE0107200).

References

[1] Su X L, Wei P, Li H, Liu W, Yan Y G, Li P, Su C Q, Xie C J, Zhao W Y, Zhai P C, Zhang Q J, Tang X F and Uher C 2017 *Adv. Mater.* **29** 1602013
[2] Pourkiaei S M, Ahmadi M H, Sadeghzadeh M, Moosavi S, Pourfayaz F, Chen L G, Pour Y M A and Kumar R 2019 *Energy* **186** 115849
[3] Li D L, Gong Y N, Chen Y X, Lin J M, Khan Q, Zhang Y P, Li Y, Zhang H and Xie H P 2020 *Nano-Micro Lett.* **12** 36
[4] Xia X G, Zhang Q, Zhou W B, Xiao Z J, Xi W, Wang Y C and Zhou W Y 2021 *Chin. Phys. B* **30** 078801
[5] Xu S D, Shi X L, Dargusch M, Di C A, Zou J and Chen Z G 2021 *Prog. Mater. Sci.* **121** 100840
[6] Deng L and Chen G M 2021 *Nano Energy* **80** 105448
[7] Chen G M, Xu W and Zhu D B 2017 *J. Mater. Chem. C* **5** 4350
[8] Prunet G, Pawula F, Fleury G, Cloutet E, Robinson A J, Hadziioannou G and Pakdel A 2021 *Mater. Today Phys.* **18** 100402
[9] Wang L M, Zhang Z M, Liu Y C, Wang B R, Fang L, Qiu J J, Zhang K and Wang S R 2018 *Nat. Commun.* **9** 3817
[10] Wang H, Ail U, Gabrielsson R, Berggren M and Crispin X 2015 *Adv. Energy Mater.* **5** 1500044
[11] Ansari M A, Mohiuddin S, Kandemirli F and Malik M I 2018 *RSC Advances* **8** 8319
[12] Xiao S Q, Zhang Q Q and You W 2017 *Adv. Mater.* **29** 1601391
[13] Liu Y, Ogawa K and Schanze K S 2009 *J. Photoch. Photobiol. C* **10** 173
[14] Lu K and Liu Y Q 2010 *Curr. Org. Chem.* **14** 2017
[15] Li J, Wang H Y, Li Y, Zhang Q Y and Jia Y 2016 *Acta Phys. Sin.* **65** 103101 (in Chinese)
[16] Joo Y, Huang L F, Eedugurala N, London A E, Kumar A, Wong B M, Boudouris B W and Azoulay J D 2018 *Macromolecules* **51** 3886
[17] Li B Z, Li X X, Yang F, Chen Y J, Mao X H, Wan S X, Xin H, Yan S T, Wang M L, Gao C M and Wang L 2021 *ACS Appl. Energy Mater.* **4** 4662
[18] Li H, Song J, Xiao J, Wu L L, Katz H E and Chen L D 2020 *Adv. Funct. Mater.* **30** 2004378
[19] Lee J, Kim J, Nguyen T L, Kim M, Park J, Lee Y, Hwang S, Kwon Y W, Kwak J and Woo H Y 2018 *Macromolecules* **51** 3360
[20] Beaujuge P M, Amb C M and Reynolds J R 2010 *Accounts Chem. Res.* **43** 1396
[21] Li Y F and Zou Y P 2008 *Adv. Mater.* **20** 2952
[22] Huo L J, Zhang S Q, Guo X, Xu F, Li Y F and Hou J H 2011 *Angew. Chem. Int. Ed.* **50** 9697
[23] Gao J H, Wang W, Zhang S J, Xiao S Q, Zhan C, Yang M Y, Lu X H and You W 2018 *J. Mater. Chem. A* **6** 179
[24] Lu L Y and Yu L P 2014 *Adv. Mater.* **26** 4413
[25] Lai C H, Li J J, Xiang X Z, Wang L and Liu D Q 2018 *Poly. Composit.* **39** 126
[26] Fernandes M R, Garcia J R, Schultz M S and Nart F C 2005 *Thin Solid Films* **474** 279
[27] Bubnova O and Crispin X 2012 *Energy Environ. Sci.* **5** 9345
[28] Kroon R, Mengistie D A, Kiefer D, Hynynen J, Ryan J D, Yu L Y and Müller C 2016 *Chem. Soc. Rev.* **45** 6147
[29] Zhang Q, Sun Y M, Xu W and Zhu D B 2014 *Adv. Mater.* **26** 6829
[30] Yamamoto J and Furukawa Y 2015 *J. Phys. Chem. B* **119** 4788
[31] Liu C, Yi C, Wang K, Yang Y L, Bhatta R S, Tsige M, Xiao S Y and Gong X 2015 *ACS Appl. Mater. Interfaces* **7** 4928

[32] Mai C K, Schlitz R A, Su G M, Spitzer D, Wang X, Fronk S L, Cahill D G, Chabinyc M L and Bazan G C 2014 *J. Am. Chem. Soc.* **136** 13478
[33] Shi K, Zhang F J, Di C A, Yan T W, Zou Y, Zhou X, Zhu D B, Wang J Y and Pei J 2015 *J. Am. Chem. Soc.* **137** 6979
[34] Furukawa Y, Akiyama K, Enokida I and Yamamoto J 2016 *Vib. Spectrosc.* **85** 29
[35] Hu Y J, Liu X F, Jiang F X, Zhou W Q, Liu C C, Duan X M and Xu J K 2017 *J. Phys. Chem. B* **121** 9281
[36] Jung I H, Hong C T, Lee U H, Kang Y H, Jang K S and Cho S Y 2017 *Sci. Rep.* **7** 44704
[37] Scholes D T, Yee P Y, Lindemuth J R, Kang H, Onorato J, Ghosh R, Luscombe C K, Spano F C, Tolbert S H and Schwartz B J 2017 *Adv. Funct. Mater.* **27** 1702654
[38] Enengl C, Enengl S, Pluczyk S, Havlicek M, Lapkowski M, Neugebauer H and Ehrenfreund E 2016 *ChemPhysChem* **17** 3836
[39] Fukuda T, Toda A, Takahira K, Kuzuhara D and Yoshimoto N 2017 *Org. Electron.* **48** 96
[40] Noh J, Jeong S and Lee J Y 2016 *Nat. Commun.* **7** 12374
[41] Grey J, Thomas A and Gao J 2015 *SPIE Nanoscience + Engineering*, August 20, 2015, San Diego, California, USA, p. 95490V
[42] Razzell-Hollis J, Tsoi W C and Kim J S 2013 *J. Mater. Chem. C* **1** 6235
[43] Razzell-Hollis J, Wade J, Tsoi W C, Soon Y, Durrant J and Kim J S 2014 *J. Mater. Chem. A* **2** 20189
[44] Kim T Y, Kim J E and Suh K S 2006 *Poly. Inter.* **55** 80
[45] Heon K S, Heo S, Ihn S G, Yun S, Hwan P J, Chung Y, Lee E, Park G and Yun D J 2014 *Appl. Phys. Lett.* **104** 243303
[46] Sabbatini L, Malitesta C, De G E, Losito I, Torsi L and Zambonin P G 1999 *J. Electron Spectrosc. Relat. Phenom.* **100** 35
[47] Kettle J, Ding Z, Horie M and Smith G C 2016 *Org. Electron.* **39** 222
[48] Jeong J, Seo J, Nam S, Han H, Kim H, Anthopoulos T D, Bradley D D and Kim Y 2016 *Adv. Sci.* **3** 1500269
[49] Bakshi A K and Ladik J 1988 *Solid State Commun.* **65** 1203
[50] Das M and Ramasesha S 2006 *J. Chem. Sci.* **118** 67
[51] Darlatt E, Muhsin B, Roesch R, Lupulescu C, Roth F, Kolbe M, Gottwald A, Hoppe H and Richter M 2016 *Nanotechnology* **27** 324005
[52] Prasad K S, Rao A, Chauhan N S, Bhardwaj R, Vishwakarma A and Tyagi K 2018 *Appl. Phys. A* **124** 98
[53] Liu J, Garman M P, Dong J J, Van D Z B, Qiu L, Portale G, Hummelen J C and Koster L J A 2019 *ACS Appl. Energy Mater.* **2** 6664